Extension of Multiband Opacity-Binning to Molecular, Non-Boltzmann Shock Layer Radiation

Christopher O. Johnston,

NASA Langley Research Center, Hampton, VA 23681

Amal Sahai and Marco Panesi

University of Illinois at Urbana-Champaign, Urbana, IL 61801

I. Nomenclature

$B_{\nu,j}$	Blackbody function for at ν_j, erg-cm^{-2}/sr
c	Speed of light, 2.9979×10^{10} cm/s
h	Planck's constant, 6.6256×10^{-27} erg-s
$\tilde{j}_i$	Emission coefficient for opacity bin i, W/cm^3-sr
J_i	Emission term for opacity bin i, W/sr
K_i	Absorption cross section, including induced emission, for bin i, cm^2
k	Boltzmann constant, 1.3806×10^{-16} erg/K
$N_{Molecule}$	Total number density for the molecule of interest, particles/cm^3
N_{bands}	Number of frequency bands
N_{bins}	Number of opacity bins for each frequency band
$N_{freq,bands}$	Number of frequency points included in each frequency band
$N_{freq,bins}$	Number of frequency points included in each opacity bin
$q_{h\nu}$	Frequency-dependent radiative flux, W/cm^2-eV
$\tilde{q}_{k,i}$	Radiative flux from frequency band k and opacity bin i, W/cm^2
T_x	Temperature, where x=e,v, or r for electronic, vibrational, or rotational modes, K
$\tilde{\kappa}_i$	Absorption coefficient, including induced emission, for bin i, cm^{-1}
ν	Frequency, s^{-1}

ϕ	Non-Boltzmann number density ratio defined in text
$\sigma_{\nu,j}$	Absorption cross section including induced emission for frequency point j, cm^2

II. Introduction

For accurate predictions of shock layer radiative heating to reentry vehicles, the smeared rotational band (SRB) model [1, 2] is appropriate for molecular band systems with negligible self absorption, meaning they are optically-thin. However, for band systems with noticeable self absorption, the orders-of-magnitude more computationally expensive line-by-line (LBL) approach is required [3]. Considering past and proposed NASA missions, the molecular band systems most likely to require the LBL approach are the CO 4th-Positive, CN Violet, and CO_2 IR bands. The CO 4th-Positive and CN Violet bands are required for Mars entry at velocities greater than 6 km/s [4], with the CN Violet band also required for Titan entry [3]. These two bands typically emit strongly in flow regimes with non-Boltzmann upper electronic state populations. The CO_2 IR band is required for Mars entry at velocities below 5 km/s [5, 6]. This ro-vibrational band system is typically assumed to contain Boltzmann populations of radiating levels (the quality of this assumption is the subject of other studies [7]).

The LBL requirement for modeling the CO 4th-Positive and CN Violet bands is restrictive because the non-Boltzmann computation of electronic states, which impacts the emission and absorption of these bands, depends on nonlocal escape factors [8]. These nonlocal escape factors require multiple iterative radiative transport evaluations for a single line-of-sight, therefore, multiplying the computational cost by the number of iterations required (usually around 5), which becomes excessively high for the LBL approach. For the CO_2 IR band, the LBL requirement is restrictive because this band system is the dominant radiator in the afterbody region of Mars entry vehicles [5]. Radiative flux computations in these afterbody regions require the ray-tracing approach [9], which involves more than 500 line-of-sight radiative transport evaluations to compute the radiative flux to a single surface point, compared to the single evaluation required for the tangent-slab approach commonly applied to forebody surface points.

The preceding paragraphs motivate the development of an orders-of-magnitude more efficient alternative to the LBL approach for the three molecular band systems identified. Such an alternative approach would also need to meet the three following requirements. For application to NASA flight programs, the approach should reproduce the LBL radiative flux prediction to within 2% for conditions where the band system provides a noticeable contribution to the total radiative flux. Furthermore, the approach must be applicable to non-Boltzmann electronic state populations to accommodate the CO 4th-Positive and CN Violet bands. Finally, the approach must be embeddable within a radiation computation that also contains a line-by-line model for atomic lines, detailed photoionization cross sections, as well as an SRB model for other optically-thin molecular band systems.

The multiband opacity binning (MBOB) approach, developed by Wray et al. [10] and Scoggins et al. [11] meets the above requirements, although it has been previously applied only for Boltzmann conditions. The purpose of this Note is therefore to extend the MBOB approach, which is reviewed in Section III, to non-Boltzmann conditions. This extension to non-Boltzmann conditions is presented in Section IV. The accuracy of the developed non-Boltzmann MBOB approach is then demonstrated in Section V for the CO 4th-Positive, CN Violet, and CO_2 IR band systems. This Note shows that the MBOB approach consistently produces radiative heating values within 2% of the LBL approach with two orders-of-magnitude less computational time.

III. Opacity Binning for Boltzmann Molecular Band Systems

The opacity binning approach presented by Wray et al. [10] divides the spectrum into a relatively small (10 - 100) number of bins depending on their absorption coefficient (or opacity). Scoggins et al. [11] extended this approach by dividing the spectrum into frequency bands, and then defining a separate bin model within each band. This approach by Scoggins et al. is the multiband opacity binning (MBOB) approach pursued in this work. The primary benefit of the MBOB approach is that it reduces the ≈500,000 spectral points required by the LBL approach to the equivalent expense of roughy 2,000 spectral points (equal to the number of bins times the number of frequency bands). This reduction is performed once and saved in tables as a function of T_{ve}, T_{tr}, and pressure. These

tables are then interpolated within the radiation code to the properties along a line-of-sight. The reduction in the number of spectral points reduces proportionally the number of radiative transport evaluations performed by the radiation code, which reduces the computational time by roughly two orders of magnitude.

The first step in developing an MBOB model for a given molecular band system is to obtain the LBL absorption coefficient spectrum for a range of T_{ve}, T_{tr}, and pressure, assuming Boltzmann distributions. The total frequency range of this spectrum is then divided into the desired number of frequency bands (N_{bands}). A given frequency band k is defined by all frequency points ν_j (from the full LBL computation) that are located within the minimum and maximum frequency limits $\nu_{min,k}$ and $\nu_{max,k}$. Next, each frequency point j in frequency band k is assigned to a bin i depending on its absorption cross section $\sigma_{\nu,j}$, as described in the next paragraph. This bin assignment is performed for a single reference condition, and then fixed for the later computation of bin properties over a range of temperatures and pressures. For the present study, the reference pressure was set to 0.1 atm and the reference temperature ($T_{ve} = T_{tr}$) was set to 8,000 K for CO 4th-Positive and CN Violet and 3,000 K for CO_2 IR. These conditions were chosen to approximately match typical shock layer conditions. However, the accuracy of the MBOB approach was found to be relatively insensitive to the applied reference condition.

Following Scoggins et al. [11], frequency points are assigned to bins by forcing an equal number of frequency points into each bin ($N_{freq,bin}$). This is in contrast to previous approaches, which predefined $\sigma_{\nu,j}$ intervals and then assigned frequency points to each bin, which may lead to many unfilled bins. To assign each frequency point from the LBL computation to a bin, the reference condition values of $\sigma_{\nu,j}$ are sorted in ascending order for each frequency band k. The sorted $\sigma_{\nu,j}$ space is then separated equally into the desired number of bins (N_{bins}), therefore, assigning an equal number of frequency points into each bin. Figure 1 presents an example of bins defined for a frequency band with $h\nu_{min,k}$ and $h\nu_{max,k}$ of 6.9 and 7.3 eV, respectively (for clarity, only 10 bins are used in this example, whereas 50 are used for the final model). Each symbol is a frequency point j from the LBL computation. This figure shows that because bin limits were chosen indirectly by enforcing an equal number of frequency points in each bin, the range of $\sigma_{\nu,j}$ values for each bin

varies.

Once each ν_j is assigned to the kth band ($p_{band}(j) = k$) and ith bin ($p_{bin}(j) = i$), then the emission term (equal to the emission coefficient divided by the molecule's number density) for each bin is computed assuming Boltzmann emission and summing over all ν_j in the bin:

$$J_i = \sum_{j \in G_i} \sigma_{\nu,j} B_{\nu,j} \Delta\nu_j \tag{1}$$

where the Planck function is defined as:

$$B_{\nu,j} = \frac{2h{\nu_j}^3}{c^2(e^{\frac{h\nu_j}{kT_{ve}}} - 1)} \tag{2}$$

The absorption cross section is obtained from J_i and $B_{\nu,j}$ as follows:

$$K_i = \frac{J_i}{\sum_{j \in G_i} B_{\nu,j} \Delta\nu_j} \tag{3}$$

For a Boltzmann population of electronic states, the emission and absorption coefficients for each bin i are written as:

$$\tilde{j}_i = J_i N_{Molecule} \tag{4}$$

and

$$\tilde{\kappa}_i = K_i N_{Molecule} \tag{5}$$

where $N_{Molecule}$ is the total number density for the molecule of interest. These equations will be extended to non-Boltzmann conditions in the next section. The radiative transfer equations are evaluated for each bin, using $\tilde{j}_i$ and $\tilde{\kappa}_i$, identically to the frequency points for the LBL approach. The only difference is that the frequency integrated radiative intensity or flux is obtained by summing over all bins and bands, instead of numerically integrating over frequency.

The advantage of the MBOB approach is that there are only $N_{bands} \times N_{bins}$ values for J_i and K_i required to model the spectrum of the given molecular band system for a given T_{ve}, T_{tr}, and pressure. The present work applies values of N_{bands} =30 and N_{bins} =50, resulting in 1,500 values for each J_i and K_i, which is significantly less than the 500,000 required for the LBL approach. For the present work, tables were compiled for 100 K increments in T_{ve} ranging from 3,000 to 12,000 K for CO 4th-Positive and CN Violet and 300 to 6,000 K for CO_2 IR. This relatively small ΔT_{ve}

is required because of the exponential T_{ve} dependence in Eq. 2. However, the T_{tr} dependence is relatively weak, limited mostly to its impact on line broadening, which allows ΔT_{tr} values of 3,000 K to be used. Furthermore, the T_{tr} values are computed as ΔT_{ve} increments away from T_{ve}, which assures that $T_{ve} = T_{tr}$ values, which are present throughout the majority of the shock layer, are accurately captured. The shock layer pressures of present interest are below 1 atm, which results in negligible pressure broadening for CO 4th-Positive and CN Violet bands. This observation allows the pressure dimension to be removed when compiling the J_i and K_i tables. For CO_2 IR, however, pressure broadening is noticeable for the present range of conditions. This is because CO_2 IR is located at much lower values of ν, which results in the ν^{-2} dependence of pressure broadening to reach the same order-of-magnitude as doppler broadening, which has a ν^{-1} dependence. The pressure dependence for CO_2 IR is captured with only 2 pressures, at 0.1 and 1.0 atm.

IV. Extending Opacity Binning for Non-Boltzmann Electronic States

The J_i and K_i values derived in the previous section assume that the LBL values for $\sigma_{\nu,j}$ are computed assuming a Boltzmann distribution of electronic, vibrational, and rotational states for a single molecular band system. The present section allows $\tilde{j}_i$ and $\tilde{\kappa}_i$ to be computed for non-Boltzmann electronic states using the previously compiled J_i and K_i values. This approach maintains Boltzmann vibrational levels at T_{ve} and rotational levels at T_{tr}.

To assess the non-Boltzmann computation, it is convenient to define the following term:

$$\phi = \frac{N_U}{N_L} \frac{N_L^{Boltz}}{N_U^{Boltz}} \tag{6}$$

where N_U and N_L are the upper and lower electronic state populations of the molecular band system, respectively, and the "Boltz" superscript represents their values assuming a Boltzmann distribution. Hence, for Boltzmann electronic state populations of N_U and N_L, the resulting ϕ is equal to unity. For the post-shock flows of present interest, N_U is lower than N_U^{Boltz}, and N_L is approximately equal to N_L^{Boltz}, which results in ϕ less than unity. From Eqs. (4) and (6), the emission coefficient for bin i may be written for non-Boltzmann electronic state populations as:

$$\tilde{j}_i = J_i \phi \frac{N_L}{N_L^{Boltz}} N_{Molecule} \tag{7}$$

Similarly, the absorption coefficient for bin i is written as:

$$\tilde{\kappa}_i = K_i \frac{1 - \phi e^{-\frac{h\tilde{\nu}_k}{kT_e}}}{1 - e^{-\frac{h\tilde{\nu}_k}{kT_e}}} \frac{N_L}{N_L^{Boltz}} N_{Molecule} \tag{8}$$

Note that the $\tilde{\nu}_k$ values in this equation are the midpoint value for the frequency band k, which is a required approximation because of the use of spectral bins and bands. This dependence indicates an advantage of treating many frequency bands, which reduces the range of ν_j values in each bin, which makes $\tilde{\nu}_k$ closer to the exact value.

While the focus of this study is to demonstrate the accuracy of the MBOB approach for an isolated non-Boltzmann molecular band systems, it should be noted that this approach can be embedded within a radiation code that treats a conventional spectrum. This conventional spectrum may include detailed photoionization cross sections, line-by-line treatment of atomic lines, and SRB models for optically thin molecular band systems. The hybrid approach is achieved by evaluating the radiative transport equations once using the MBOB values for $\tilde{\kappa}_i$ and once using the conventional spectrum. These two evaluations are coupled by adding the absorption coefficient from the conventional spectrum, averaged over each frequency band k, to the MBOB values for $\tilde{\kappa}_i$ (for all bins). Similarly, the absorption coefficient for the conventional spectrum is altered by adding $\sum_i \tilde{\kappa}_i$ as a constant over each frequency band. These changes to the conventional and MBOB absorption coefficients are performed prior to the radiative transport evaluations. The resulting radiative flux values from each evaluation are combined to provide the total radiative flux.

V. Results and Comparisons

This section compares the results of the MBOB approach with the LBL approach for the CO 4th-Positive, CN Violet, and CO_2 IR band systems. Mars entry conditions are considered for the CO 4th-Positive and CO_2 IR band comparisons, while Titan entry is considered for the CN Violet comparisons (CN Violet is present in the Mars simulations, however, its Titan contribution contains more self absorption, and is therefore a more challenging test for the MBOB approach). The flowfield simulations are performed using the LAURA v5 Navier-Stokes solver [12]. For Mars entry, a two-temperature thermochemical nonequilibrium model with 16 species (CO_2, CO, N_2, O_2, NO, C, N, O, CN, C_2, C^+, O^+, NO^+, O_2^+, CO^+, and e^-) is applied, using the kinetic rates presented

by Johnston and Brandis [13]. For Titan entry, a two-temperature thermochemical nonequilibrium model with 18 species (CH_4, CH_3, CH_2, CH, NH, H, H_2, N_2, N_2^+, C, N, CN, C_2, N^+, C^+, H^+, Ar, and e^-) is applied, using the the kinetic rates presented by Gocken [14]. The non-Boltzmann rates presented by Johnston and Brandis are applied for both CO 4th-Positive and CN Violet. For simplicity, all simulations are performed for an axisymmetric hemisphere, with 32 grid points along the surface and 128 shock clustered points in the body normal direction. Also for simplicity, coupled radiation is not included and the tangent-slab approach is applied to compute the radiative flux. These simplifications should not impact the relative comparison between the MBOB and LBL approaches, which is the focus of this work. Note that for all cases presented in this Section, the MBOB approach is two orders-of-magnitude more computationally efficient than the LBL approach.

A. CO 4th-Positive

To assess the accuracy of the MBOB approach relative to the LBL approach for modeling non-Boltzmann CO 4th-Positive radiation, Mars entry conditions similar to Pathfinder [15] were chosen. These conditions consist of a velocity of 7 km/s for all cases, with free-stream densities ranging from 5×10^{-5} to 5×10^{-4} kg/m^3. Nose radii of 0.5 and 5.0 m are considered to model, respectively, a smaller entry probe (such as Pathfinder) and a larger vehicle, such as a hypersonic aerodynamic decelerator (HIAD) [16]. Figure 2 presents the percent error, relative to the LBL approach, in the stagnation point radiative heating predicted by the MBOB and SRB models. To accentuate the differences between the results of these approaches, only CO 4th-Positive is considered in the radiative heating computation. As mentioned in the Introduction, the SRB approach is a computationally efficient approach that is only appropriate for band systems with negligible self absorption, meaning they are optically-thin. The greater than 5% error for the SRB approach shown in this figure indicates that the CO 4th-Positive band is not optically-thin for these cases. This non-optically-thin regime is required to make a meaningful assessment of the SRB or MBOB approaches, because for optically-thin conditions, both approaches would agree essentially exactly with the LBL approach. Thus, the SRB results are presented throughout the following discussion to demonstrate that the conditions are not optically-thin, and to show that the MBOB approach

predicts more accurate results than the SRB approach with similar computational efficiency (note that the percent error under the assumption of an optically-thin radiative flux is greater than 100% for all cases presented in Fig. 2, so that actually, the SRB approach captures the non-optically-thin behavior reasonably well with its less than 20% error). In this regard, Figure 2 shows that the MBOB results are within 1.5% of the LBL approach for all cases. Note that these results are for the stagnation point. Peak differences for the MBOB approach of 3.5% are present near the shoulder (for the SRB approach, the difference is up to 50%), where the radiative heating due to this band system is 4 orders of magnitude lower than at the stagnation point. At these locations, the CO 4th-Positive band contributes less than 20% of the total radiative flux (CO IR and CN Red dominate). Therefore, this 3.5% error in the CO 4th-Positive contribution results in less than a 1% error in the total radiative flux, which is within the desired accuracy.

To further investigate the ability of the MBOB approach to accurately reproduce the LBL results, a 0.5 m radius case at 7 km/s and a density of 2×10^{-4} kg/m^3 is considered in detail. Figure 3 presents the stagnation point temperature profiles for this case. This figure shows a noticeable region of thermal nonequilibrium between 2.2 and 2.6 cm, while the entire shock layer is in chemical nonequilibrium. Values of ϕ range from 0.2 at the peak T_{ve} location to roughly 0.5 throughout the rest of the layer, indicating that CO 4th-Positive is non-Boltzmann at these conditions.

Wall-directed radiative flux profiles predicted by LBL, MBOB, and SRB approaches are compared in Fig. 4. The LBL and MBOB results are nearly coincident, and are therefore difficult to distinguish, whereas the SRB approach predicts a noticeably larger radiative flux resulting from the post-shock nonequilibrium region. Figure 5 compares the stagnation point radiative flux spectrum resulting from the three approaches. The thin lines represent the spectrum and the thick lines represent the cumulative integrated value. For clarity, the LBL spectrum is averaged over 0.02 eV increments. Again, the LBL and MBOB cumulative results are nearly coincident. This figure shows that, unlike the SRB approach, the MBOB approach is capable of accurately predicting the Planck-limited region of the spectrum between 7 and 10 eV. Note that the step-like appearance of the MBOB spectrum is the result of a single radiative flux value being computed for each of the

N_{bands} (equal to the sum of the bin values in each band). However, if the band (k) and bin (i) of each frequency point j are saved (as $p_{band}(j) = k$ and $p_{bin}(j) = i$) when constructing the MBOB model, then the spectrum may be reconstructed in detail through the following equation:

$$q_{h\nu,j} = \tilde{q}_{p_{band}(j),p_{bin}(j)} \frac{N_{freq,band}}{N_{freq,bin}} \frac{1}{(\nu_{max,p_{band}(j)} - \nu_{min,p_{band}(j)})} \tag{9}$$

where $\tilde{q}_{p_{band}(j),p_{bin}(j)}$ is the radiative flux resulting from the bin and band associated with this spectral point j. Figure 6 compares the reconstructed MBOB spectrum with the LBL spectrum over a limited spectral range (for clarity). This figure shows that the 50 bins of the MBOB model are able to capture the details of the LBL spectrum. The frequency band shown here, which uses the same 50 bins, extends 14 times the $h\nu$ range shown in the figure. Within this spectral range there are 10,000 spectral points for the LBL approach. Therefore, the radiative transfer equation is evaluated 10,000 times for the LBL approach and only 50 times for the MBOB approach for this frequency band. Nevertheless, the MBOB approach is able to capture the spectral details shown in this figure.

B. CN Violet

To demonstrate the MBOB approach for non-Boltzmann CN Violet emission, Titan entry cases at 7 km/s are considered, with free-stream densities ranging from 5×10^{-5} to 5×10^{-4} kg/m^3, and nose radii of 0.5 and 5.0 m. Figure 7 presents the percent error, relative to the LBL approach, in the stagnation point radiative heating (due to CN Violet only) predicted by the MBOB and SRB models. The MBOB approach is again seen to predict values within 1.5% of the LBL approach. Because of its location in the spectrum, CN Violet is less optically-thick than CO 4th-Positive. Regardless, the optically-thin radiative flux results in a 10% and 50% over-prediction for the 0.5 and 5 m cases, respectively, which indicates substantial optical thickness for these cases. Figure 8 compares the stagnation point spectrum resulting from the three approaches (the cumulative curve is multiplied by 100 to place it on the same vertical scale) for the 5 m radius case at a density of 2×10^{-4} kg/m^3. Again, the cumulative curves for the LBL and MBOB results are nearly indistinguishable. The cumulative curves indicate that the SRB approach is unable to accurately model the optically thick peak near 3.2 eV. Note that values of ϕ range from 0.8 at the peak T_{ve} location to roughly 0.95

throughout the rest of the layer, indicating that CN Violet is non-Boltzmann at these conditions.

C. CO_2 IR

The CO_2 IR band system provides significant radiative heating to Mars entry vehicles at velocities below 5 km/s. This radiative heating component is especially important in afterbody regions, where the radiative heating may be significantly larger than convective heating. To approximate the larger radiating volume present for afterbody radiation, a 5 m radius sphere is considered exclusively. Because this radiative component occurs at lower velocities, corresponding to lower altitudes in a trajectory, slightly higher densities (1×10^{-4} to 1×10^{-3} kg/m^3) than those considered in the previous examples are considered. Figure 9 presents the resulting difference in the stagnation point radiative heating. The MBOB approach is seen to agree within 0.5%, while even the SRB approach agrees within 6%. Although not shown, the errors in assuming an optically-thin radiative flux range from 30 to 180% for the 3 km/s cases and 10 to 40% for the 5 km/s cases. Again, this indicates that these cases are not optically-thin, and therefore, they provide a meaningful assessment of the MBOB approach. The excellent agreement seen here between the MBOB and LBL approaches is consistent with the study of Potter et al. [17], which reported good agreement for CO_2 IR using the opacity binning approach of Wray et al. [10], which applies a single frequency band.

VI. Conclusions

The multiband opacity binning (MBOB) approach is extended to non-Boltzmann electronic state populations. Application of the MBOB approach to a range of Mars and Titan entry cases results in difference of less than 2% relative to the line-by-line (LBL) approach. The MBOB approach is over 100 times more computationally efficient than the LBL approach, making it ideal for ray-tracing and coupled radiation flowfield applications.

VII. Acknowledgments

The present work was funded by the NASA Space Technology Mission Directorate Entry Systems and Modeling (ESM) project.

VIII. References

[1] Patch, R. W., Shackleford, W. L., and Penner, S. S., "Approximate Spectral Absorption Coefficient Calculations for Electronic Bands Systems Belonging to Diatomic Molecules," *Journal of Quantitative Spectroscopy and Radiative Transfer*, Vol. 2, 1962, pp. 263–271.

[2] Chambers, L. H., "Predicting Radiative Heat Transfer in Thermochemical Nonequilibrium Flow Fields," NASA TM 4564, 1994.

[3] Johnston, C. O., Hollis, B. R., and Sutton, K., "Radiative Heating Methodology for the Huygens Probe," *Journal of Spacecraft & Rockets*, Vol. 44, No. 5, 2007, pp. 993–1002.

[4] Johnston, C. O., Brandis, A. M., and Sutton, K., "Shock Layer Radiation Modeling and Uncertainty for Mars Entry," AIAA Paper 2012–2866, 2012.

[5] Brandis, A. M., Saunders, D. A., Johnston, C. O., Cruden, B. A., and White, T. R., "Radiative Heating on the After-Body of Martian Entry Vehicles," AIAA Paper 2015–3111, 2015.

[6] West, T. K., Theisinger, J., Brune, A. J., and Johnston, C. O., "Backshell Radiative Heating on Human-Scale Mars Entry Vehicles," AIAA Paper 2017–4532, 2017.

[7] Sahai, A., Lopez, B. E., Johnston, C. O., and Panesi, M., "Novel Approach for CO_2 State-to-State Modeling and Application to Multi-Dimensional Entry Flows," AIAA Paper 2017–0213, 2017.

[8] Johnston, C. O., "Influence of Radiative Absorption on Non-Boltzmann Modeling for Mars Entry," *Journal of Thermophysics and Heat Transfer*, Vol. 28, No. 4, 2014, pp. 795–798.

[9] Mazaheri, A., Johnston, C., and Sefidbakht, S., "Three-Dimensional Radiation Ray-Tracing for Shock Layer Radiative Heating Simulations," *Journal of Spacecraft & Rockets*, Vol. 50, No. 3, 2013, pp. 485–493.

[10] Wray, A. A., Prabhu, D. K., and Ripoll, J.-F., "Opacity Distribution Functions Applied to the CEV Reentry," AIAA Paper 2007–4542, 2007.

[11] Scoggins, J. B., Magin, T. E., Wray, A., and Mansour, N. N., "Multi-Group Reductions of LTE Air Plasma Radiative Transfer in Cylindrical Geometries," AIAA Paper 2013–3142, 2013.

[12] Mazaheri, A., Gnoffo, P. A., Johnston, C. O., and Kleb, B., "LAURA Users Manual," NASA TM 2013-217800, 2013.

[13] Johnston, C. O. and Brandis, A. M., "Modeling of Nonequilibrium CO Fourth-Positive and CN Violet Emission in CO_2-N_2 Gases," *Journal of Quantitative Spectroscopy and Radiative Transfer*, Vol. 149, 2014, pp. 303–317.

[14] Gocken, T., "N_2-CH_4-Ar Chemical Kinetic Model for Simulations of Titan Atmospheric Entry," *Journal of Thermophysics and Heat Transfer*, Vol. 21, No. 1, 2007, pp. 9–18.

[15] Willcockson, W. H., "Mars Pathfinder Heatshield Design and Flight Experience," *Journal of Spacecraft & Rockets*, Vol. 36, No. 3, 1999, pp. 374–379.

[16] Brune, A. J., West, T. K., Hosder, S., and Edquist, K. T., "Uncertainty Analysis of Mars Entry Flows over a Hypersonic Inflatable Aerodynamic Decelerator," *Journal of Spacecraft & Rockets*, Vol. 52, No. 3, 2015, pp. 776–788.

[17] Potter, D., Karl, S., Lambert, M., and Hannemann, K., "Computation of Radiative and Convective Contributions to Viking Afterbody Heating," AIAA Paper 2013–2895, 2013.

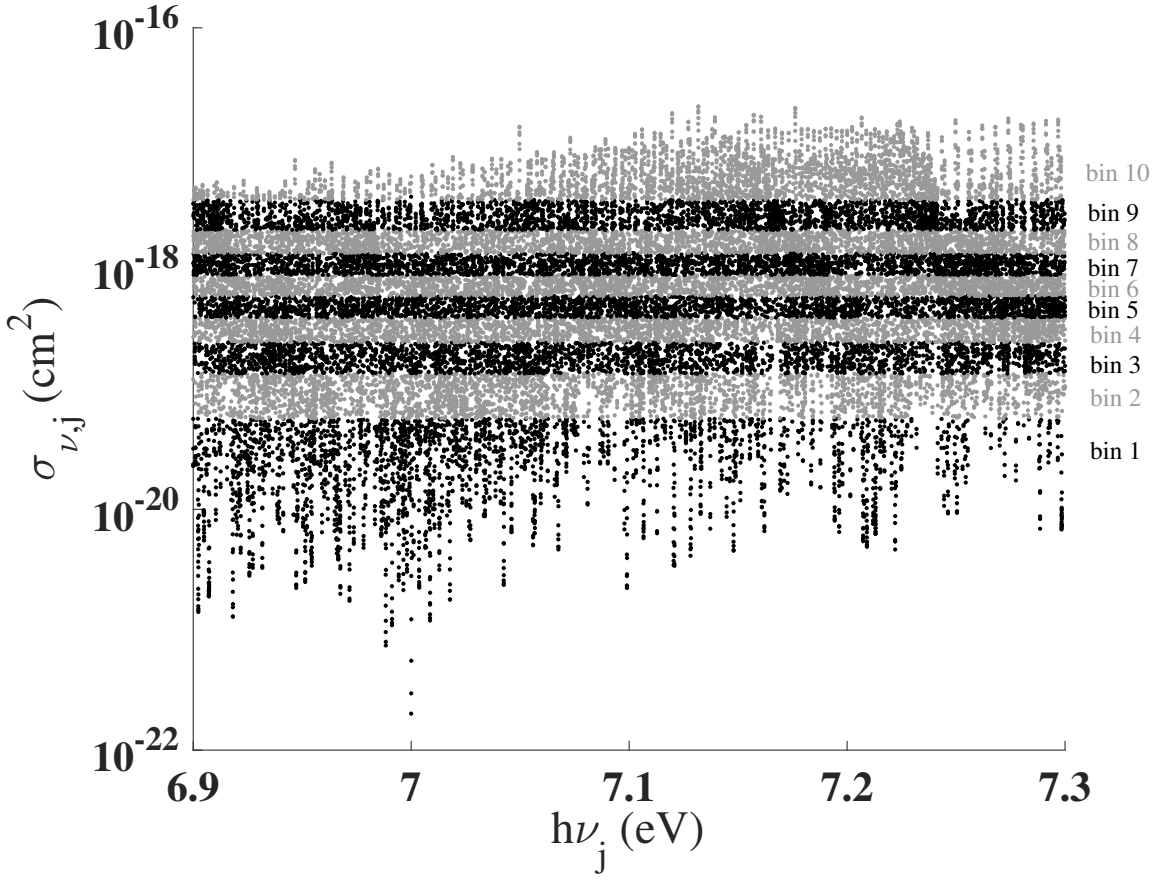

Fig. 1: Opacity bin groupings for a single frequency band.

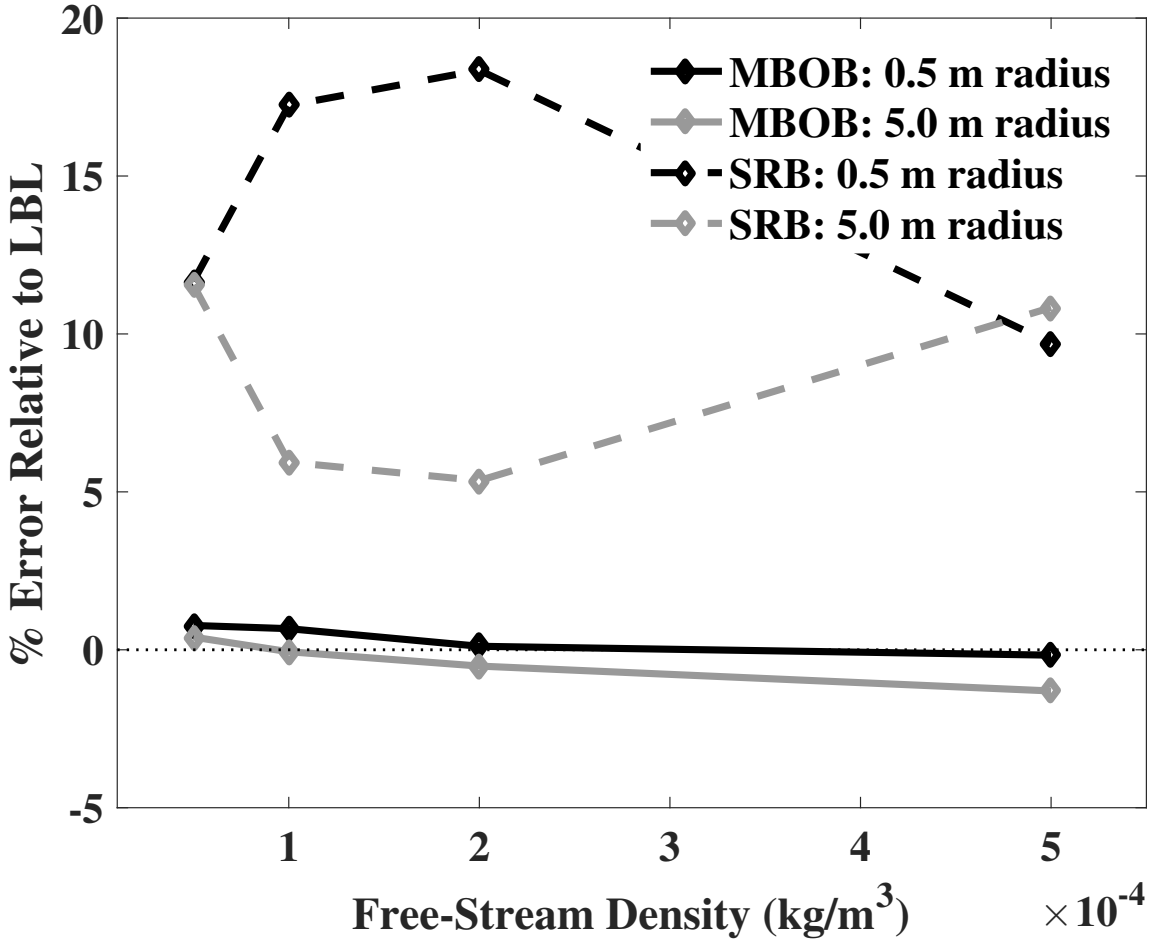

Fig. 2: Percent error in stagnation point radiative heating, relative to LBL, assuming radiation from CO 4th-Positive only.

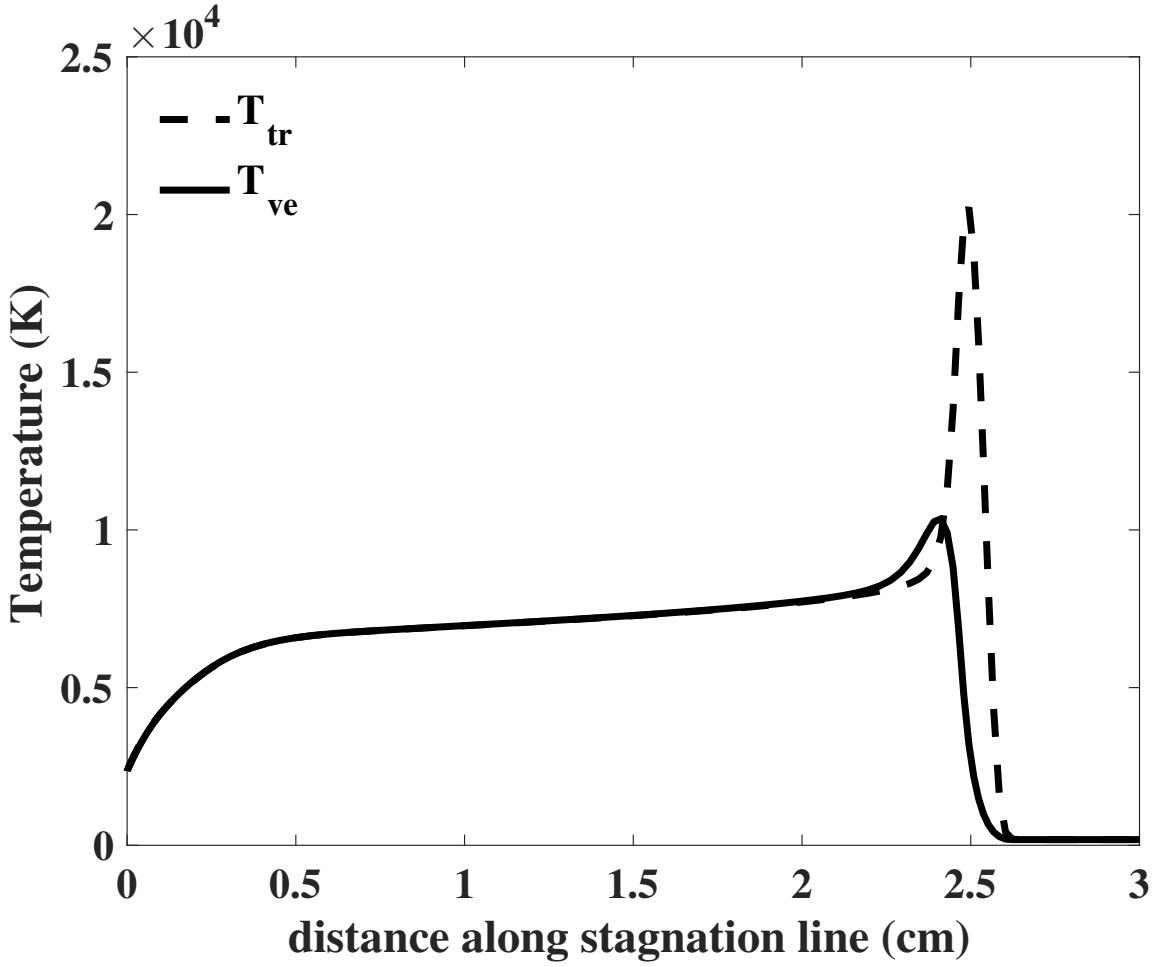

Fig. 3: Stagnation line temperature profile for Mars entry with 0.5 m nose radii and density of 2e-4 kg/m^3.

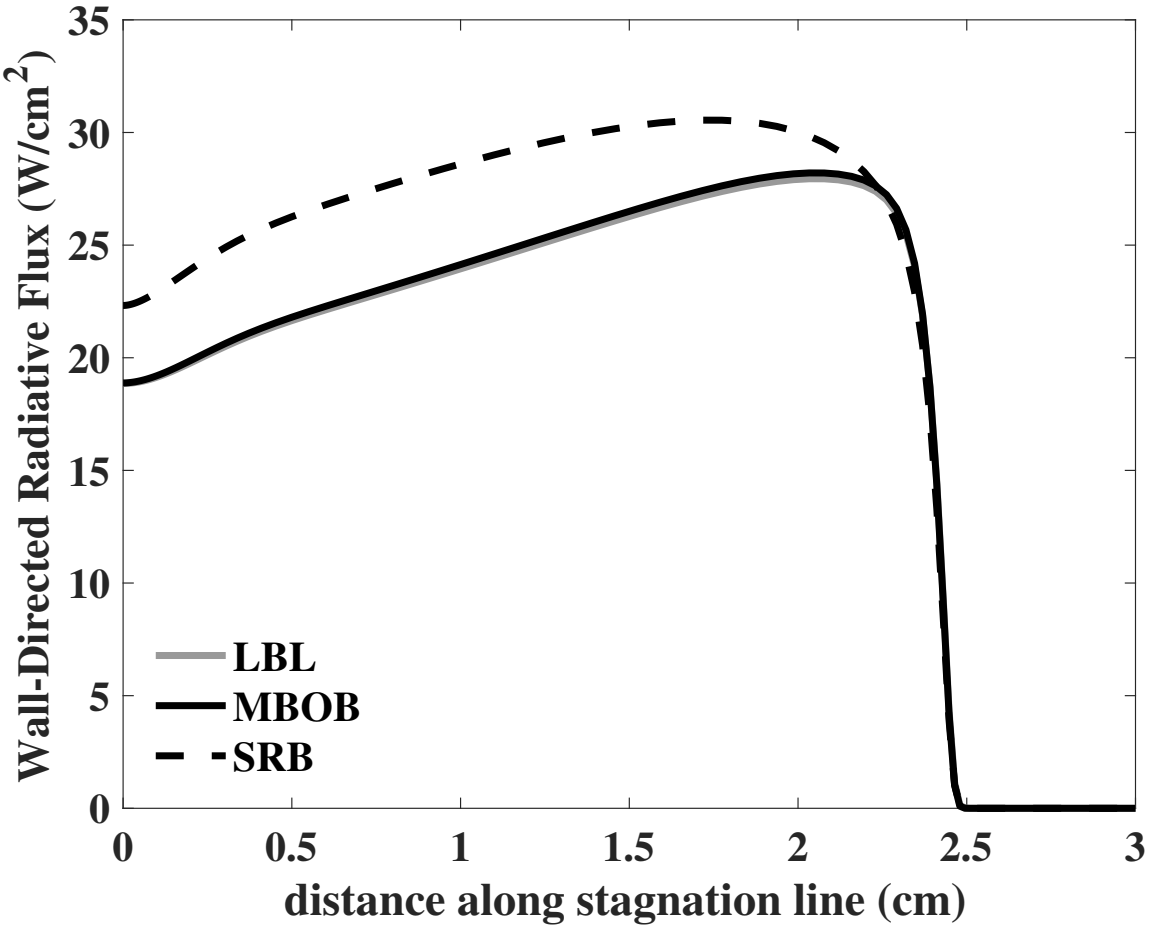

Fig. 4: Wall-directed radiative flux for Mars entry case, assuming radiation from CO 4th-Positive only.

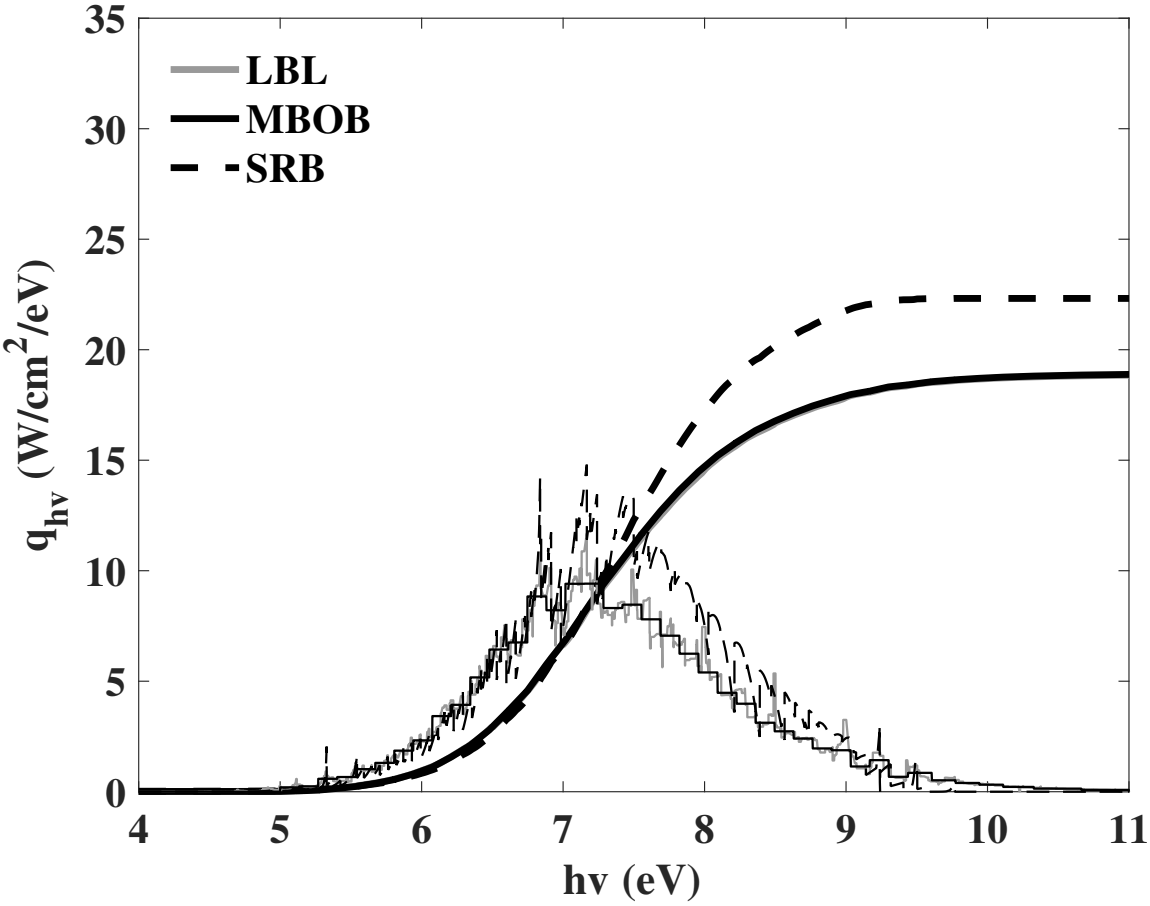

Fig. 5: Wall-directed radiative flux spectrum at the wall for the Mars entry case, assuming radiation from CO 4th-Positive only.

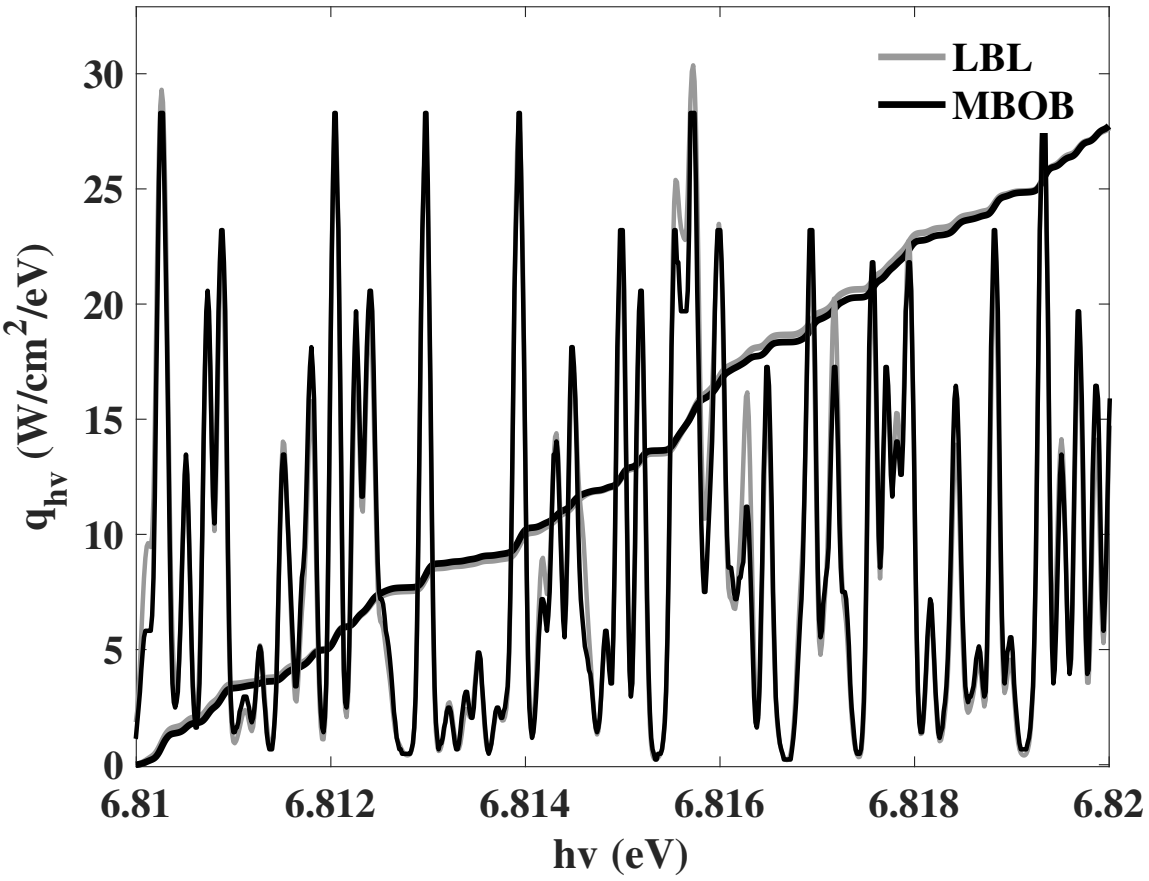

Fig. 6: Comparison of reconstructed MBOB radiative flux spectrum with LBL result.

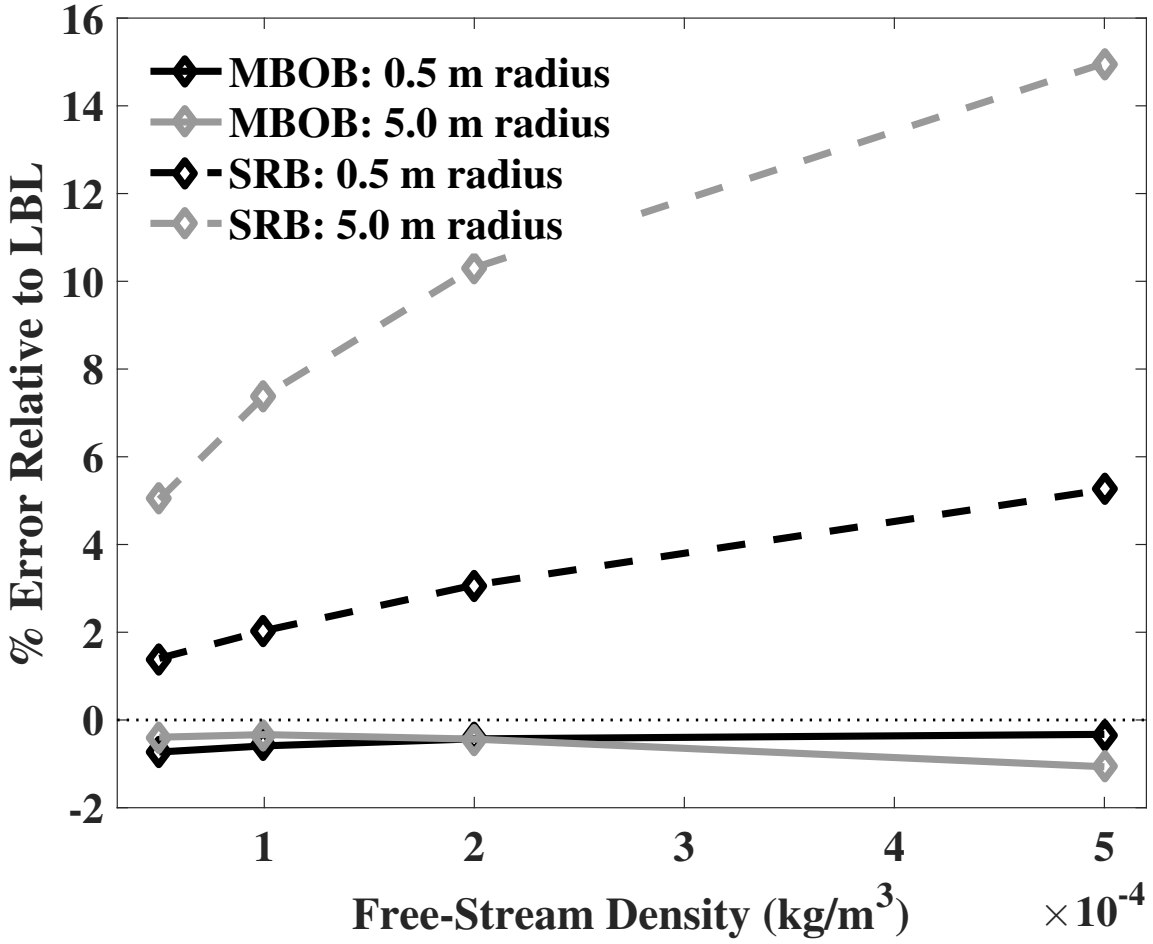

Fig. 7: Percent error in stagnation point radiative heating, relative to LBL, assuming radiation from CN Violet only.

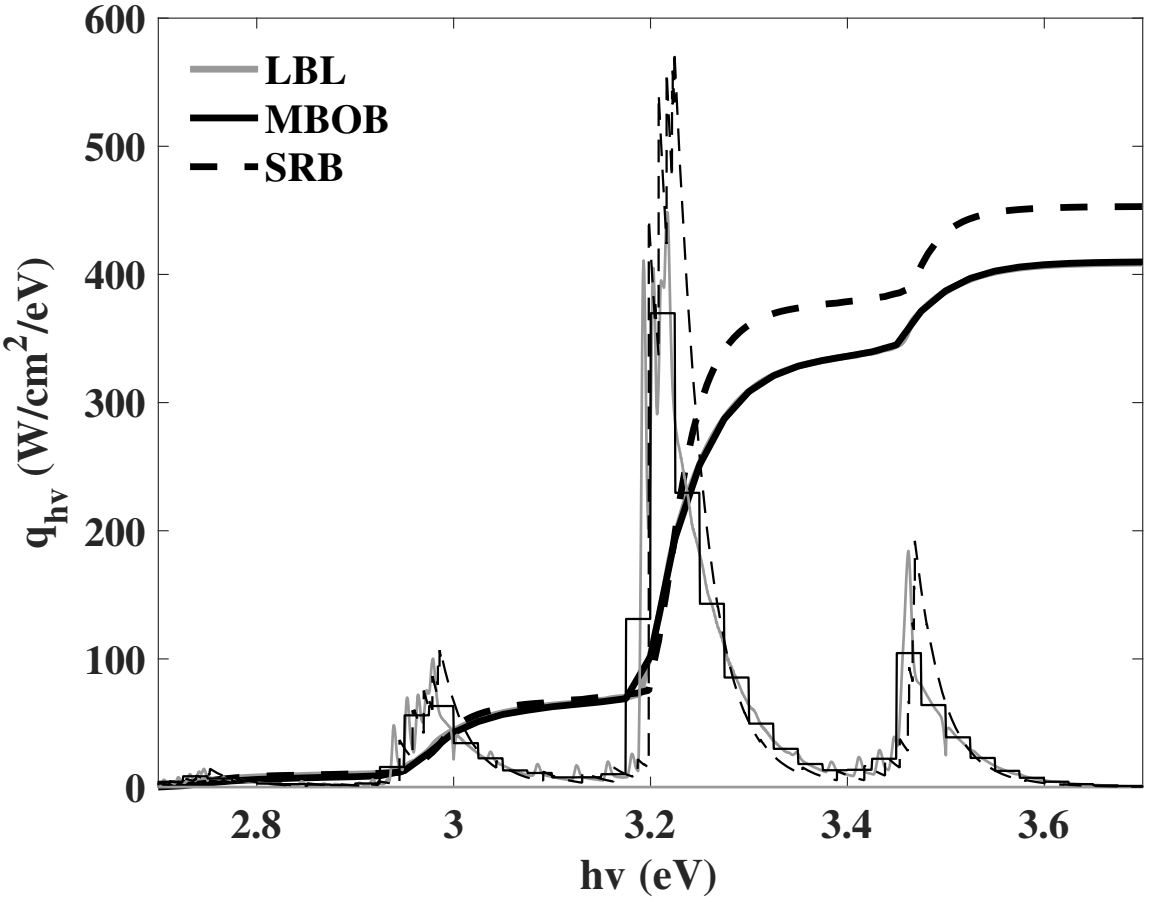

Fig. 8: Wall-directed radiative flux spectrum at the wall for the Titan entry case, assuming radiation from CN Violet only.

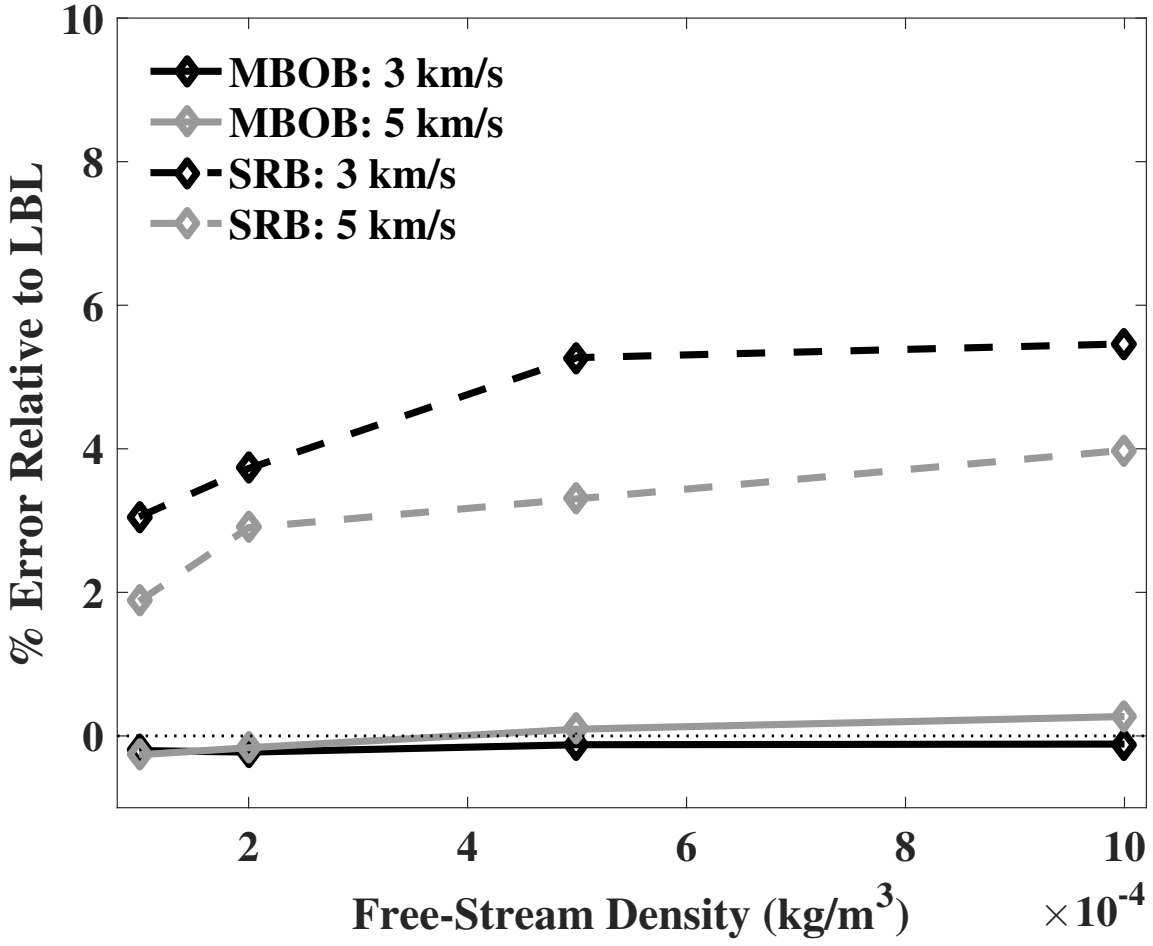

Fig. 9: Percent error in stagnation point radiative heating, relative to LBL, assuming radiation from CO_2 IR only.